A New Reaching Law for Anti-disturbance Sliding-mode Control of PMSM Speed Regulation System

Yaoqiang Wang, *Member, IEEE*, Yutao Feng, Xiaoguang Zhang, *Member, IEEE*, and Jun Liang, *Senior Member, IEEE*

***Abstract*—In this paper, in order to optimize the dynamic performance of the permanent magnet synchronous motor (PMSM) speed regulation system, a nonlinear speed-control algorithm for the PMSM control systems using sliding-mode control (SMC) is developed. First, a sliding-mode control method based on a new sliding-mode reaching law (NSMRL) is proposed. This NSMRL includes the system state variable and the power term of sliding surface function. In particular, the power term is bounded by the absolute value of the switching function, so that the reaching law can be expressed in two different forms during the reaching process. This method can not only effectively suppresses the inherent chattering, but also increases the velocity of the system state reaching to the sliding-mode surface. Based on this new reaching law, a sliding-mode speed controller (SMSC) of PMSM is designed. Then, considering the large chattering phenomenon caused by high switching gain, an improved anti-disturbance sliding-mode speed controller(ADSMSC) method, called SMSC+ESO method, is developed. This method introduces an extended state observer (ESO) to observe the lumped disturbance and adds a feedforward compensation item based on the observed disturbances to the SMSC. Finally, simulation and experimental results both show the validity of the proposed control method.**

***Index Terms*—permanent magnet synchronous motor (PMSM), anti-disturbance sliding mode speed controller (ADSMSC), new sliding-mode reaching law (NSMRL), extended state observer (ESO).**

I. INTRODUCTION

Permanent magnet synchronous motor (PMSM) has many advantages, i.e., simple structure, high power density and high efficiency. PMSM has been widely used in the fields of high precision CNC machine tools, robot, aerospace and other fields [1], [3], [8]. But at the same time, the PMSM is a complex control object with multi variable, strong coupling, nonlinear, and variable parameters [2], [3]. If the traditional linear control method such as proportional-integral (PI) is adopted, the control precision can only be met within a certain range. At the same time, the PI control method depends on the accuracy of the system model, which is highly susceptible to external disturbances and internal parameter changes. All these may make the control system deviating from the expected target [3].

Therefore, in order to solve the problems of traditional PI controller, some nonlinear control theories are proposed and developed, e.g., fuzzy control [4], auto disturbance rejection control [5], predictive control [6],[7], sliding-mode control (SMC) [8]–[10] and neural network control [11]. Among them, sliding-mode control has become a research hotspot because of its low requirement on model accuracy and strong robustness to external interference. Sliding-mode control has been successfully applied in motor speed regulation system [8], [13], [14]. A fuzzy sliding-mode speed controller applied to PMSM can be found in [12]. In [15], a hybrid control method based on sliding-mode controller was applied to the closed loop control system of PMSM, and the results are very conclusive regarding the effectiveness of the sliding-mode controller. In addition, a neural network sliding-mode control method was proposed in [16] to improve speed tracking precision.

However, the sliding-mode method is not flawless; indeed, in practical applications, there are time delays in switching control law, which leads to high-frequency dynamics, known as chattering. Thus, many alternative methods have been proposed to overcome the chattering phenomenon, such as reaching law method [10], [17], high-order sliding-mode method [18], [19], nonsingular terminal sliding-mode [20], and fractional-order sliding-mode [21]. Among them, since the reaching law method can directly act on the reaching process, it can more effectively solve the chattering problem. In [22], a practical discrete-time fractional-order terminal sliding-mode variable structure speed controller was designed. The experimental results show that the dynamic performance of the controlled system is improved. In [23], the terminal switching gain term was added on the basis of the conventional exponential approach law, and the saturation function was designed to replace the switching function. The simulation results show the effectiveness of the proposed method. [24] added the terminal attractor on the basis of the traditional reaching law, which guarantees the system still have a fast

Manuscript received xx xx, 2019; revised xx xx, 2019; accepted xx xx, 2019. Date of publication xx xx, 2019; date of current version xx xx, 2019. This work was supported in part by the National Natural Science Foundation of China under Grant 51507155, and the National Natural Science Foundation of China under Grant 51877002. Recommended for publication by Associate Editor xxxx. *(Corresponding author: Xiaoguang Zhang.)*

Yaoqiang Wang is with the School of Electrical Engineering, Zhengzhou University, Zhengzhou 450001, China (e-mail: WangyqEE@163.com).

Yutao Feng is with the Zhengzhou University, Zhengzhou 450001, China, and China Aviation Optical-Electrical Technology Co., Ltd., Luoyang 471003, China (e-mail: qqfengyutao@163.com).

Xiaoguang Zhang is with the North China University of Technology, Beijing 100144, China (e-mail: zhangxg123456789@163.com).

Jun Liang is with the Zhengzhou University, Zhengzhou 450001, China, and Cardiff University, Cardiff CF24 3AA, U.K. (e-mail: LiangJ1@cardiff.ac.uk).

Color versions of one or more of the figures in this paper are available online at http://ieeexplore.ieee.org.

Digital Object Identifier xxxxx/TPEL.xxxx.xxxx

reaching speed near the sliding-mode surface, but exists complex parameter adjusting and so on.

Conventionally, in SMC the switching gain should be set large enough to offset the system disturbance in order to guarantee strong robustness and stability of the system, i.e., the minimum switching gain must increase along with the increasing system disturbance. However, in practice, the upper bound of the system disturbance is difficult to determine; meanwhile, owing to the switching function in the control law, the large switching gain will lead to the occurrence of high-frequency sliding-mode chattering. Thus, to alleviate drawbacks above, combining the SMC with other reaches which estimate the disturbance is an attractive proposition. Recently, the nonlinear disturbance observer control methods for mismatched uncertainties [25], [26] have been thoroughly studied, which show that the mismatched disturbance can be eliminated from the output by designing the observer for the feed-forward compensation, and the system performance will not be affected simultaneously. In [27]–[30], this method has been practically tested on the robotics, the converters and the PMSM speed regulation system. The results show that, a good robustness performance can be achieved.

In this paper, in order to further improve the dynamic performance of the PMSM speed regulation system, a new reaching law is proposed. On the basis of the traditional exponential reaching law (TERL), the system state variable and the power order term of the sliding-mode function are introduced in the NSMRL. When the power term is bounded by the absolute value 1 of the switching function, the reaching law can be expressed as two different reaching forms, which can not only increase the velocity of the system state reaching the sliding surface, but also ensure the system state smoothly reaches the switching surface. Then, taking into account the effect of lump disturbance, especially load disturbance, an extended state observer (ESO) based on hyperbolic tangent function (HTF) is designed to observe the disturbance, and it is used as the feed-forward compensation part be added to the SMSC. The contributions of the paper are: 1) a speed controller based on a new sliding-mode reaching law is designed for PMSM. 2) the ESO based on HTF is introduced to the SMSC to observe the lump disturbance, instead of the traditional load torque observer. 3) the anti-disturbance sliding mode speed controller (ADSMSC) has good dynamic performance and strong disturbance rejection ability for uncertain load torque.

The rest of this paper is organized as follows. The proposed NSMRL and its performance analysis are introduced in section II. In section III, combined with PMSM mathematical model, the design process of ESO-based ADSMSC is given, and the stability proof is given. In section IV, the ESO-based ADSMSC is tested on PMSM speed regulation system, and the results are compared to traditional PI regulator. Section V finally summarizes the paper.

II. NSMRL Design and Analysis

A. Reaching Law Sliding-mode Design

The main characteristic of sliding-mode variable structure control (SMVSC) is the structure of control law and control system, which are discontinuous on the switch surface. SMVSC enables the state trajectory to reach the predetermined sliding-mode surface and converge along the sliding-mode surface to state origin. However, the stability conditions can not reflect how the system reaches the sliding-mode surface.

In contrast, reaching law method can ensure the motion phase quality of the system. Choosing an appropriate reaching law can make the system have a greater reaching speed and accelerate the dynamic response of the system when state vector is far away from the sliding-mode surface. As the sliding-mode surface is reached, its reach speed decreases to zero to guarantee the state vector stay on the surface. Fig.1 shows how this mechanism takes place in the phase plane.

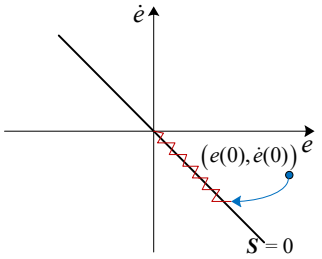

Fig.1. Sliding-mode mechanism in phase plane.

The exponent reaching law was first proposed and designed by academician Weibing Gao [31], which can be shown as

$$\frac{\mathrm{d}s}{\mathrm{d}t} = -\varepsilon\,\mathrm{sgn}(s) - ks, \quad \varepsilon>0, k>0 \tag{1}$$

where $\varepsilon\mathrm{sgn}(s)$ represents isokinetic reach term; ks represents index reach term; s is a sliding-mode surface function.

For conventional pure exponential reaching law, it can not reach the sliding-mode surface in a limit time. Therefore, the isokinetic reach term $\varepsilon sgn(s)$ is added to ensure when s is close to 0, the reaching velocity is ε instead of 0.

However, although the accessibility problem is solved by adding isokinetic reach term, the exponential reaching law reaching to the sliding-mode surface speed is determined by the design value of the parameter k, which makes it contradictory to increase the reaching speed and reduce the sliding chattering. The analysis is as follows:

In (1), when $s > 0$, it can be obtained that

$$\frac{ds}{dt} = -\varepsilon - ks \tag{2}$$

and the reaching time can be calculated by integrating (1) from 0 to t, with $s(t)=0$

$$t^* = \frac{1}{k}\left\{\ln\left[s(0)+\frac{\varepsilon}{k}\right] - \ln\frac{\varepsilon}{k}\right\} \tag{3}$$

One can see from (3) the reaching speed increases with a high value of k. Therefore, to have a faster reaching performance, k should be increased; however, a high k can lead to excessive speed when reaching the sliding surface, which will increase the chattering level. Thus, if the coefficient of the index term can be set as a variable and its value be combined with the distance between the system state point and the sliding-mode surface, the contradiction caused by the selection of

k value can be solved. This also provides an idea for proposing the new reaching law in the following paragraphs.

B. The Proposed NSMRL

The NSMRL is realized based on conventional exponential reaching law, which can adapt to the variations of the sliding-mode surface and system state. The reaching law is given by

$$\begin{cases} \dfrac{\mathrm{d}s}{\mathrm{d}t} = -\varepsilon |x|^{a} \operatorname{sgn}(s) - k |s|^{b\cdot \operatorname{sgn}(|s|-1)} s \\ \lim\limits_{t\to\infty} |x| = 0, \varepsilon > 0, k > 0, 0 < a < 1, 0 < b < 1 \end{cases} \tag{4}$$

where x represents the system state.

By analyzing the reaching law stated in (4), the following conclusions can be obtained:

If the system state is far away from the sliding-mode surface, i.e., s>1, then $sgn(|s|–1)$=1, and the system state reaches sliding-mode surface according to two rate of variable speed reaching law $\varepsilon|x|^{a}sgn(s)$ and variable index reaching law $k|s|^{b}s$. Moreover, if $|s|$ decreases, then $|s|^{b}s$ reaches 1, $k|s|^{b}s$ converges to k and $\varepsilon|x|^{a}$ converges to ε. This means that, while the system state reaches sliding-mode surface, the coefficients of the reaching law decrease gradually to restrain chattering. On the other hand, if system state is close to the sliding-mode surface, i.e., s<1, then the reaching rate of TERL will decrease to zero. On the contrary, because of the limit of absolute value sign function in new reaching law, then $sgn(|s|-1)$= -1 and the reaching velocity of the variable exponential term is $k|s|^{-b}s$, obviously there is $k|s|^{-b}s$>$k|s|^{b}s$, which increases the reaching speed of variable index reaching law.

Thus, in the whole process from the initial state to the sliding-mode surface, the reaching speed of the NSMRL is always faster than the TERL. Besides, the introduction of the system state variable and the power order term of the sliding-mode function restrain the shortcoming of chattering phenomenon.

C. Performance Analysis of NSMRL

In order to take a comparative analysis between TERL and NSMRL, a typical motor system shown in (5) is established as

$$J\ddot{\theta} = u(t) + d(t) \tag{5}$$

where J is rotary inertia; $\theta(t)$ represents position instruction; $u(t)$ represents control input; $d(t)$ represents external disturbance.

The controlled system is assumed as

$$\ddot{\theta}(t) = -f(\theta, t) + hu(t) + d(t) \tag{6}$$

where $f(\theta,\ t)$=25 $\dot{\theta}$ and h=133 are set as known conditions; $d(t)$ is set as 10sin(πt).

Assuming that θ_{d} is an ideal position signal, than the error signal e can be expressed as θ_{d}–θ. The sliding-mode surface function s is defined as

$$s = \dot{e} + ce \tag{7}$$

where c>0 satisfies the Hurwitz condition.

When the sliding-mode surface function is determined, the position tracking error and its reciprocal can be defined as

$$\begin{cases} e(t) = \theta_{\mathrm{d}} - \theta(t) \\ \dot{e}(t) = \dot{\theta}_{\mathrm{d}} - \dot{\theta}(t) \end{cases} \tag{8}$$

where $\theta_{\mathrm{d}}(t)$ is an ideal position signal.

Next, combining (5), (6), (7) and (8), it can be obtained that

$$\begin{aligned} \dot{s}(t) &= c\dot{e}(t) + \ddot{e}(t) \\ &= c\left[\dot{\theta}_{\mathrm{d}} - \dot{\theta}(t)\right] + \left[\ddot{\theta}_{\mathrm{d}} - \ddot{\theta}(t)\right] \\ &= c\left[\dot{\theta}_{\mathrm{d}} - \dot{\theta}(t)\right] + \left[\ddot{\theta}_{\mathrm{d}} + f(\theta, t) - hu - d\right] \end{aligned} \tag{9}$$

Based on the new reaching law, according to (4) and (9), the improved sliding-mode control rate is given by

$$\begin{aligned} u(t) = \frac{1}{h}[&\varepsilon |x|^{a} \operatorname{sgn}(s) + k |s|^{b\operatorname{sgn}(|s|-1)} s \\ &+ c(\dot{\theta}_{\mathrm{d}} - \dot{\theta}) + \ddot{\theta} + f(\theta, t)] \end{aligned} \tag{10}$$

Using MATLAB s function, a simulation is carried out among TERL, the reaching law in reference [8] (RLR8) and NSMRL, and the simulation parameters are set as follows: c=15，ε=10，k=20，a=0.5 and b=0.3. The system ideal position signal θ_{d} is set as sin(t). The initial state of the controlled object $\boldsymbol{x}(0)$ is set as [x_1, x_2]=[-2, -2].

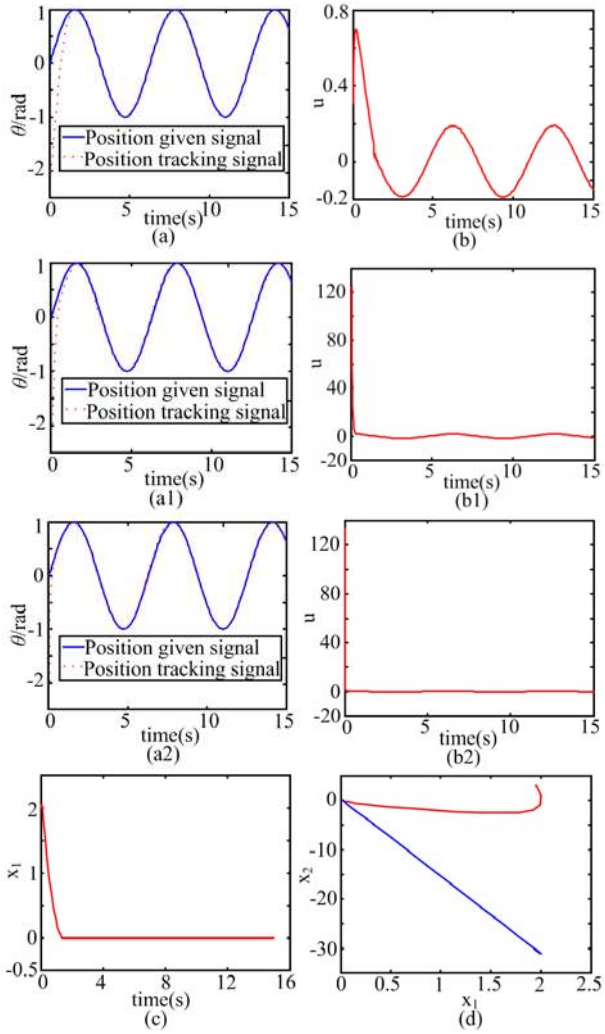

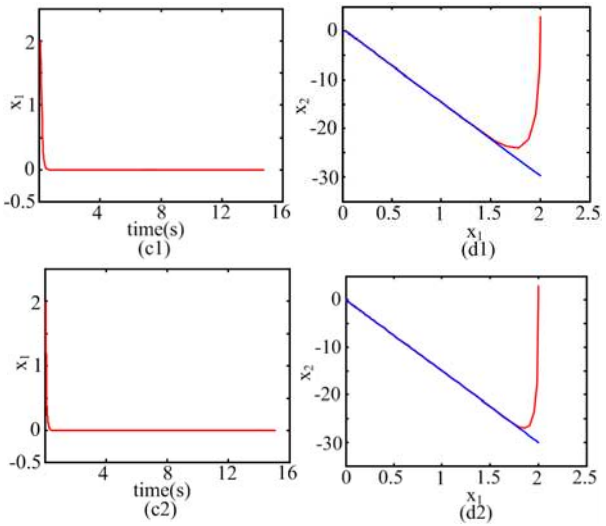

Fig.2. Performance comparison among TERL, the reaching law in reference [8] (RLR8) and NSMRL. (a) Tracking performance of TERL. (a1) Tracking performance of the RLR8. (a2) Tracking performance of NSMRL. (b) Controller output of TERL. (b1) Controller output of the RLR8 (b2) Controller output of NSMRL. (c) Position error convergence rate of TERL. (c1) Position error convergence rate of the RLR8. (c2) Position error convergence rate of NSMRL. (d) Phase trajectory of TERL. (d1) Phase trajectory of the RLR8. (d2) Phase trajectory of NSMRL.

Fig.2 shows the performance comparison diagram among TERL, the reaching law in reference [8] (RLR8) and NSMRL. We can get the conclusions that the NSMRL is obviously superior to the TERL in tracking given signal, reducing the position tracking error, improving the differential convergence speed of the position tracking error and restraining the chattering. Moreover, the NSMRL can track without delay and overshoot. Therefore, compared with the RLR8, the NSMRL proposed in this paper has the advantages of faster reaching speed and better stable controller output effect.

D. The Discrete form of NSMRL

In practical engineering applications, the real time computer control is a discrete control system. Due to the inherent characteristics of discrete control, the existence, accessibility and stability of the sliding mode are different from that of the continuous system. Thus, in this section, from the viewpoint of discrete, the discrete form of the proposed NSMRL is given when the sliding-mode surface is near to 0 and the performance is compared with TERL in the discrete state.

In discrete system, the sliding-mode surface function is designed as

$$s(k) = Cx(k) \tag{11}$$

where $C = [c_1 \ \dots \ c_n]$ and c_n=1.0.

Next, the switching band that surrounding the switching surface is represented as

$$S^{\Delta} = \left\{ x \in R^n \mid -\Delta < s(x) = cx < +\Delta \right\} \tag{12}$$

It needs to be explained that the sliding state of discrete systems starting from any initial state can be divided into two types after reaching the sliding surface in finite step: 1) reaching the sliding-mode surface s and moving on it; 2) moving in the switching band and step through the switching surface at every step. The two types above shown in Fig.3 are referred to as quasi-sliding-mode of discrete variable structure control.

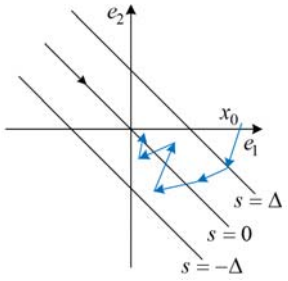

Fig.3. Quasi-sliding-mode diagram

If the sliding-mode surface s is near to 0, the proposed NSMRL in (4) can be simplified as $ds/dt \approx -\varepsilon|x|^a sgn(s)$. Its discrete expression is expressed as

$$s(n+1) - s(n) = -\varepsilon T |x|^a \operatorname{sgn}(s(n)) \tag{13}$$

where T represents the sampling period.

Assuming that the system motion trajectory reaches the sliding-mode surface in finite step, which implies that $s(n)=0^+$ or $s(n)=0^-$, then the equation of the next period can be obtained with $s(n)=0^+$:

$$s(n+1) = -\varepsilon T |x|^a \tag{14}$$

Similarly, when $s(n)=0^-$, the next periodic equation is

$$s(n+1) = \varepsilon T |x|^a \tag{15}$$

according to (14) and (15), the thickness ζ of the discrete sliding-mode band for (13) is

$$\zeta = 2\varepsilon T |x|^a \tag{16}$$

also, when the sliding-mode surface s approximated to 0, the TERL reaching velocity is determined by isokinetic reach term and the discrete form is as follows:

$$s_1(n+1) - s_1(n) = -\varepsilon_1 T \operatorname{sgn}(s_1(n)) \tag{17}$$

Then again, the thickness ζ_1 of the discrete sliding-mode band for (17) is

$$\zeta_1 = 2\varepsilon_1 T \tag{18}$$

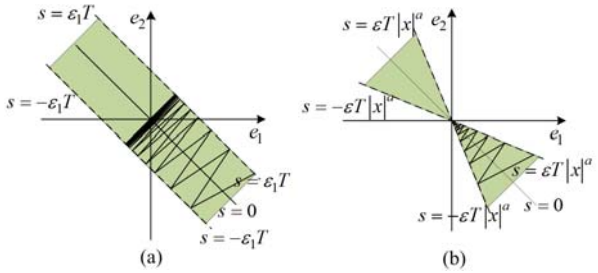

Fig.4. Comparison of state trajectories between TERL and NSMRL.

By analyzing (18), as shown in Fig.4 (a), the switching bandwidth of TERL is a fixed value, which makes the system state fail to reach the equilibrium origin (0,0) stably, but tend to be the chattering between $(-\varepsilon_1 T, \varepsilon_1 T)$; In contrast, because of the power term of state variable is introduced in (16), as shown in Fig.4 (b), which can make the system converge to the equilibrium origin (0,0) steadily under the control law.

Besides, this advantage also provides a possibility for speed controller designed in following section to eliminate speed tracking error.

III. Design of Anti-disturbance Sliding-mode Speed Controller Based on NSMRL

A. PMSM Mathematical Model

The stator current equation of the PMSM speed control system in the d-q rotating coordinate system is expressed as

$$\begin{cases} \dfrac{di_d}{dt} = \left(u_d - Ri_d - e_d\right)/L \\ \dfrac{di_q}{dt} = \left(u_q - Ri_q - e_q\right)/L \end{cases} \tag{19}$$

where u_d , u_q and i_d , i_q represent the voltages and currents of *d*- and *q*- axis, respectively; R represents the stator resistance; L represents the stator inductance. e_d and e_q represent the motor back electromotive force, respectively.

$$\begin{cases} e_d = -\omega_e L_q i_q \\ e_q = \omega_e \left(L_d i_d + \psi_f\right) \\ \omega_e = p\omega_r \end{cases} \tag{20}$$

where L_d and L_q represent d- and q- axis inductances; ω_e and ω_r represent electrical angular velocity and mechanical angular velocity, respectively; p is the pole number of the motor.

The mechanical motion equation of PMSM is written as

$$J\frac{d\omega_r}{dt} = T_e - B\omega_r - T_L \tag{21}$$

where J represents moment of inertia; T_L represents load torque; B represents viscosity coefficient; T_e represents electromagnetic torque, and for surface-mount PMSM, the electromagnetic torque t can be expressed as

$$T_e = 1.5p\psi_f i_q \tag{22}$$

B. Design of ADSMSC with ESO

The SMC is essentially a kind of switching control. In general, the required switching gain value must be larger than the upper bound of the lumped disturbances. Thus, if the disturbances are observed and then are feed-forward compensated, the required switching gain just needs to be larger than the upper bound of the disturbance compensation error, which is usually much smaller than that of the lumped disturbance, such that the system chattering will be reduced effectively. Based on this, this paper proposes an anti-disturbance sliding mode speed controller (ADSMSC) with disturbance observation and compensation capability instead of the conventional PI speed controller to improve the dynamic performance of the system.

When considering the influence of parameter uncertainties, the equation of motion of a PMSM can be expressed as

$$\dot{\omega}_r = \left(\chi + \Delta\chi\right)i^*_q - \left(\eta + \Delta\eta\right)\omega_r - \left(\gamma + \Delta\gamma\right)T_L \tag{23}$$

where $\chi = 3n_p^2\Psi_f/2J$; $\eta = B/J$; $\gamma = n_p/J$; $\Delta\chi$, $\Delta\eta$, and $\Delta\gamma$ represent the motor parameter change values, respectively.

Selecting the parameters g and d, and their expression is as follows

$$\begin{cases} g = \Delta\chi i_q - \Delta\eta\omega_r - \Delta\gamma T_L \\ d = \chi\left(i_q - i^*_q\right) - \eta\omega_r - \gamma T_L \end{cases} \tag{24}$$

Then, the equation (23) can be rewritten as

$$\dot{\omega}_r = \chi i^*_q + g + d \tag{25}$$

among them, g is estimated by adaptive law, and the load disturbance d is observed by ESO and feedforward to obtain better control effect.

Assume that the first-order system state equation is expressed as

$$\begin{cases} \dot{x}_1(t) = f\left(x_1\right) + hu(t) \\ y(t) = x_1(t) \end{cases} \tag{26}$$

where h is a constant greater than zero; $f(x_1)$ represents a bounded nonlinear perturbation function; $u(t)$ is the control input.

If $x_2(t)$ is chosen as the expansion variable and $x_2(t) = f(x_1)$, i.e., $\dot{x}_2(t) = w(t)$, then system (26) can be expanded as

$$\begin{cases} \dot{x}_1(t) = x_2(t) + hu(t) \\ \dot{x}_2(t) = w(t) \\ y(t) = x_1(t) \end{cases} \tag{27}$$

In (27), if $u(t) = i^*_q$ and $x_1(t) = \omega_r$, by combining (25), (26) and (27), the ESO of PMSM control system based on hyperbolic tangent function (HTF) can be obtained as

$$\begin{cases} e_1(t) = z_1(t) - \omega_r(t) \\ \dot{z}_1(t) = z_2(t) + g + \chi i^*_q - \beta_1 e_1(t) \\ \dot{z}_2(t) = -\beta_2 \tanh\left(\beta_3 e_1(t)\right) \end{cases} \tag{28}$$

As known from reference [28], the speed feedback signal of PMSM is observed by z_1, and the load disturbance torque d is observed by z_2. Based on these, compensation of disturbances can be achieved. In addition, according to the principle of parameter selection in reference [28], parameters β_1, β_2 and β_3 can be selected to satisfy $\beta_1 - \beta_2\beta_3 > 0$.

Next, the speed tracking error is defined as

$$e = \omega^*_r - \omega_r \tag{29}$$

where ω^*_r represents the given speed reference value; ω_r represents the actual speed.

Then the variation law of speed tracking error equation can be expressed as

$$\dot{e} = \dot{\omega}^*_r - \chi i^*_q - g - d \tag{30}$$

In this paper, the speed tracking error e is taken as an independent variable, and the integral sliding surface is selected as

$$s = e + c\int_0^t e(\tau)\,d\tau \quad c > 0 \tag{31}$$

What needs to be explained here is that the reason for how to select the correlation between the system state variable and the reach speed is as follows. $x = e$ is selected as state variable, which represents the speed tracking error. For the speed con-

trol system, the speed tracking error is an important performance evaluation index. Therefore, choosing x as the state-associated amount with the reach speed can directly affect the error information on the sliding-mode reach speed, so that when the speed tracking error is large, the reach speed is relatively large, and vice versa. In this way, the purpose of accelerating the reaching velocity and meanwhile reducing system chattering can be achieved.

To sum up, combining the designed new reaching law (4) with (30) and (31), the output signal of speed loop controller, i.e. q-axis current reference value can be obtained as

$$i^*_q = \frac{1}{\chi}\left[\dot{\omega}^*_r - \hat{g} - d + \varepsilon|x|^a \operatorname{sgn}(s) + k|s|^{b\cdot\operatorname{sgn}(|s|-1)}s + ce\right] \quad (32)$$

where $-d/\chi$ represents the feedforward compensation part of ESO; $\hat{g}$ is the estimated value of the parameter uncertainty, which is updated according to the adaptive law shown in (33).

$$\dot{\hat{g}} = -\eta s \quad \eta > 0 \quad (33)$$

C. Stability Proof

Defining the parameter estimation error as $\tilde{g} = g - \hat{g}$, and having $\dot{\tilde{g}} = -\dot{\hat{g}}$, then, the Lyapunov function can be constructed as

$$V = \frac{1}{2}s^2 + \frac{1}{2}\cdot\frac{1}{\eta}\tilde{g}^2 \quad (34)$$

Combining (4), (30) and (33), the derivation of (34) can be obtained as

$$\begin{aligned}\dot{V} &= s\dot{s} + \frac{1}{\eta}\tilde{g}\dot{\tilde{g}} = s\left(\dot{e} + ce\right) + \frac{1}{\eta}\tilde{g}\dot{\tilde{g}} \\ &= s\left(\dot{\omega}^*_r - \chi i^*_q - g - d + ce\right) + \frac{1}{\eta}\tilde{g}\dot{\tilde{g}} \\ &= -s\left[\varepsilon|x|^a \operatorname{sgn}(s) + k|s|^{b\cdot\operatorname{sgn}(|s|-1)}s\right] + \\ &\quad s[\dot{\omega}^*_r - \chi i^*_q - \hat{g} - d + ce + \varepsilon|x|^a \operatorname{sgn}(s) + \\ &\quad k|s|^{b\cdot\operatorname{sgn}(|s|-1)}s] - \tilde{g}s - \frac{1}{\eta}\tilde{g}\dot{\tilde{g}} \\ &= -s\left[\varepsilon|x|^a \operatorname{sgn}(s) + k|s|^{b\cdot\operatorname{sgn}(|s|-1)}s\right] \le 0\end{aligned} \quad (35)$$

When the parameter selection satisfies $\varepsilon > 0$, $k > 0$, $0 < a < 1$ and $0 < b < 1$, then $\dot{V} \le 0$ is established. It is known from the Lyapunov stability theorem that the designed sliding-mode controller is progressively stable.

IV. Simulation and Implementation Verification

In this section, to demonstrate the effectiveness of ADSMSC based on NSMRL, the simulations and experiments of PI controller and the ADSMSC in one PMSM system were carried out. The block diagram of PMSM speed-regulation system is shown as Fig.6.

It should be noted that when using the standard PI algorithm for the speed controller for comparison here, it is very difficult to guarantee a good closed-loop performance in different conditions, either large overshoots for fast responses or small overshoots but with slow responses. Therefore, an antiwindup PI algorithm [32] is employed here for the speed loop. Please note that when no confusion will arise, in the following descriptions, we simply refer such antiwindup PI controller as PI controller. The main idea of this antiwindup strategy can be described as follows:

$$e_1(k) = \omega^*_r(k) - \omega_r(k) \quad (36)$$

If $i^*_q(k-1) > I_{q\max}$, then

$$\alpha = \begin{cases} 0, & e_1(k) > 0 \\ 1, & e_1(k) < 0 \end{cases} \quad (37)$$

If $i^*_q(k-1) < -I_{q\max}$, then

$$\alpha = \begin{cases} 0, & e_1(k) < 0 \\ 1, & e_1(k) > 0 \end{cases} \quad (38)$$

If $-I_{q\max} \le i^*_q(k-1) \le I_{q\max}$, then $\alpha = 1$.

$$i^*_q(k) = \mathrm{k}_p * e_1(k) + k_i * \sum_{i=0}^{k} \alpha e_1(k) \quad (39)$$

The motor parameters used in this simulation are given in Table I.

TABLE I
PARAMETERS OF THE MOTOR

Parameter and unit	Value
Rated power P_n/kW	0.4
Inductance $L_d = L_q$/mH	6.71
Flux linkage of permanent magnets Ψ_a/Wb	0.175
Stator phase resistance R/Ω	1.55
Viscous friction coefficient B/N·m·s	0.000 3
Rotational inertia J/kg·m^2	0.000 2

A. Simulation Verification

Using the PMSM vector control structure with $i_d = 0$, a simulation model was built using Matlab/Simulink.

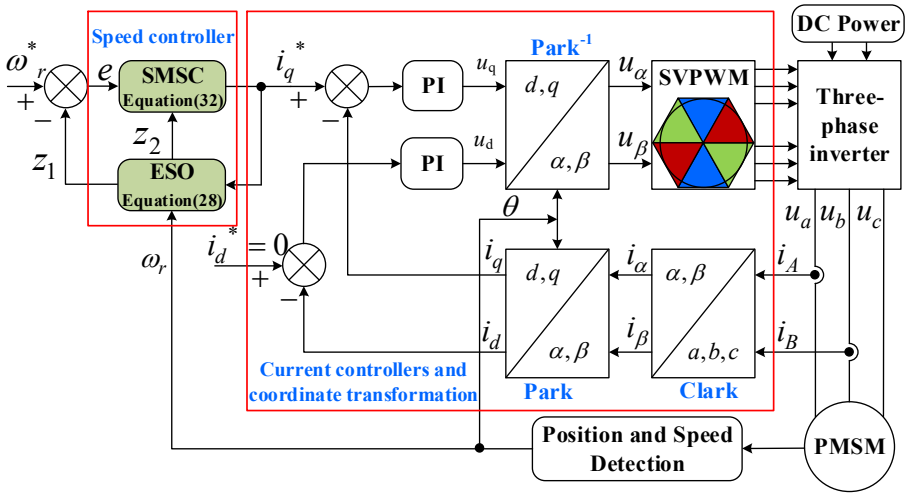

Fig.5. Block diagram of PMSM speed-regulation system.

The simulation block diagram of PMSM speed regulation system based on SMSC+ESO is shown in Fig.5. As can be seen from the figure, ESO estimates the load disturbance and compensates the results to SMSC, while the SMSC replaces the PI controller in the conventional speed loop.

The simulation is divided into two groups, and the simulation parameters are set as follows. For group one, the simulation time t is set to 0.4 s, and the given speed is 1000 r/min. The group one simulation results are shown in Fig.6 (a) and Fig.7 (a). For the other group, the simulation time t is also set to 0.4 s. In order to verify the dynamic response of the load disturbances, the motor starts with no-load torque, and when running to 0.2 s, the load torque suddenly increases to 1.27 N·m, and at 0.3 s, the load torque is discharged to 0.65 N·m. The group two simulation results are shown in Fig. 6 (b)-(d) and Fig.7 (b)-(d). Moreover, the PI parameters of both current loops are the same as: $k_{pc} = 1.1$， $k_{ic} = 0.06$. The PI parameters of the speed loop is that proportional gain $k_p = 0.11$, the integral gain $k_i = 15$ and $\alpha_0 = 0.998$ .The parameters of the SMSC+ESO controller are: a =0.6, b =0.3, c =20, ε = 5, k = 23, $\beta_1 = \beta_2 = 160$, $\beta_3 = 0.85$.

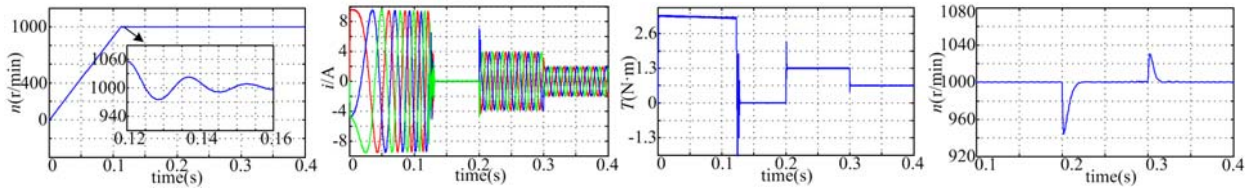

Fig.6. Simulation results of dynamic response of startup and load mutation under PI control. (a) Speed (b) Three-phase current (c) Torque change in the case of load disturbances (d) Speed fluctuation in the case of load disturbances

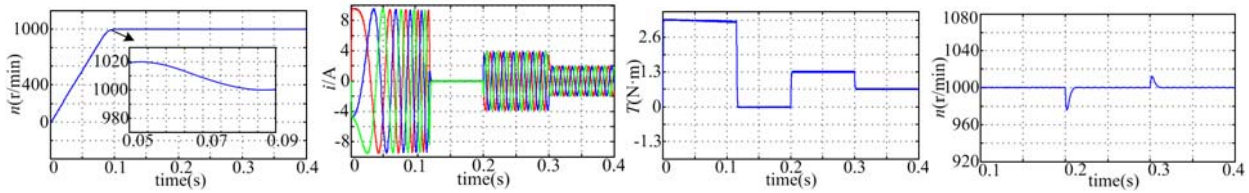

Fig.7. Simulation results of dynamic response of startup and load mutation under SMSC+ESO control. (a) Speed (b) Three-phase current (c) Torque change in the case of load disturbances (d) Speed fluctuation in the case of load disturbances

From the simulation results shown in Fig.6 (a) and Fig.7 (a), we can draw the following conclusions. Compared to the speed regulation system controlled by PI, the SMSC based on the NSMRL has a shorter settling time to reach the stable running state, and achieves the steady state almost without overshoot. In contrast, the speed regulation system under PI control has a bigger overshoot.

As shown in Fig.6 (b)–(d), it can be seen that when the external disturbance added at 0.2s and removed at 0.3s, the speed and electrical magnetic torque fluctuations are obvious. On the contrary, as shown in Fig.7 (b)–(d), when using the SMSC+ESO controller based on NSMRL, the system has better dynamic performance. The electromagnetic torque almost has no fluctuation, and the motor speed change at 0.2s is smaller, less than 20 r/min.

Therefore, from the analysis above we can draw the conclusion that the system with SMSC+ESO controller based on NSMRL has the advantages of good dynamic performance and strong robustness.

B. Experimental Verification

In order to further verify the theoretical analysis and the

proposed control method, a PMSM drive control experiment platform based on TMS320F28335 as the main control chip was set up, which mainly verifies the dynamic response of the speed regulation system under the PI controller, the SMSC with the reaching law in reference [8] (SMSC+RLR8) and the proposed SMSC+ESO controller.

The PI parameters of two current loops are the same: the proportional gain $k_{pc} = 1$, and the integral gain $k_{ic} = 0.058$. The parameters of the speed loop is that $k_p = 0.15$, $k_i = 15$, and $\alpha_0 = 0.998$. The parameters of SMSC+ESO are: $x = x_1$, $a = 0.45$, $b = 0.65$, $c = 20$, $\varepsilon = 5$, $k = 23$. $\beta_1 = \beta_2 = 160$, $\beta_3 = 0.94$. The experimental motor parameters are as follows: rated power 0.4kW, bus voltage 110V, rated current 2.6A, rated speed 3 000r/min, rated torque 1.27 N·m.

The experiment hardware platform is shown in Fig.8.

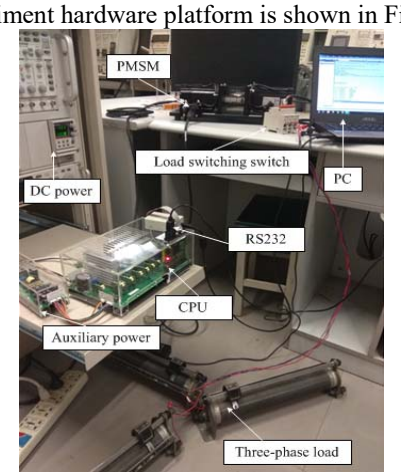

Fig.8. Experimental hardware platform

In order to verify dynamic performance of NSMRL, the first experiment was carried out to show the startup procedure of the motor when the reference speed was given as 1000 r/min with an initial load torque of 0 N·m.

The startup comparison results under different control strategies, i.e. (PI, SMSC+RLR8, SMSC+NSMRL) are shown in Fig.9 (a)–(c). Comparing Fig.9 (a) with Fig.9 (b) and (c), it is obvious that when the PI controller is adopted, the startup procedure speed fluctuation in Fig.9 (a) is very obvious, and the dynamic settling time is about 300 ms, which is longer than using SMSC. In addition, as can be seen from Fig.9 (c), the startup procedure of the system almost has no overshoot after adopting the NSMRL. Moreover, the speed settling time of SMSC+NSMRL shown in Fig.9 (c) is about 100 ms, which is shorter than adopting reaching law in RLR8.

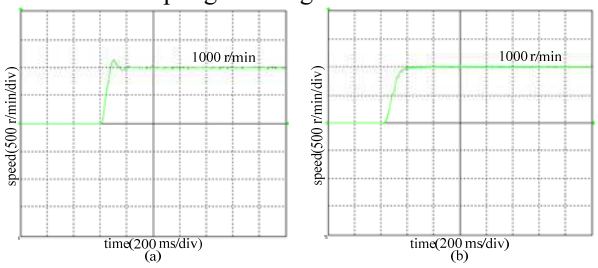

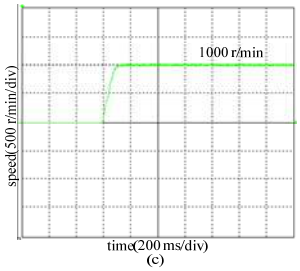

Fig.9. Startup experiment contrast under different control strategies. (a) Experimental results under PI controller. (b) Experimental results under SMSC using the reaching law in reference [8] (RLR8). (c) Experimental results under SMSC using NSMRL.

The second experiment was carried out to verify the robustness of the speed control system under the three control strategies (PI, SMSC, SMSC+ESO) when the motor is running at a steady state of 1000 r/min and a lower speed of 150 r/min.

Fig.10, Fig.11 and Fig.12 show the dynamic responses of motor speed when the load torque is added to 1.27 N·m suddenly.

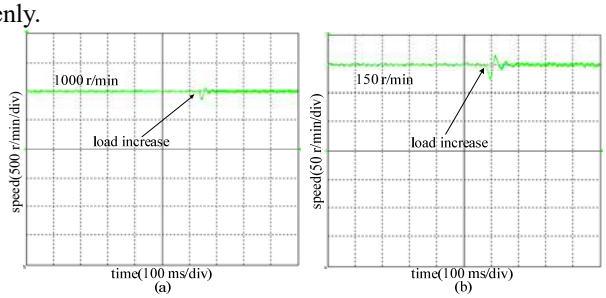

Fig.10. Experimental results under PI controller. (a) Speed (1000 r/min) in the case of sudden load increase. (b) Speed (150 r/min) in the case of sudden load increase.

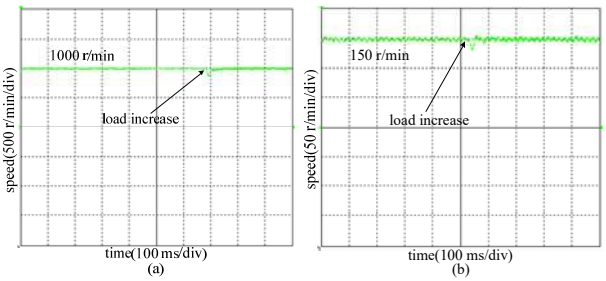

Fig.11. Experimental results under SMSC adopting NSMRL. (a) Speed (1000 r/min) in the case of sudden load increase. (b) Speed (150 r/min) in the case of sudden load increase.

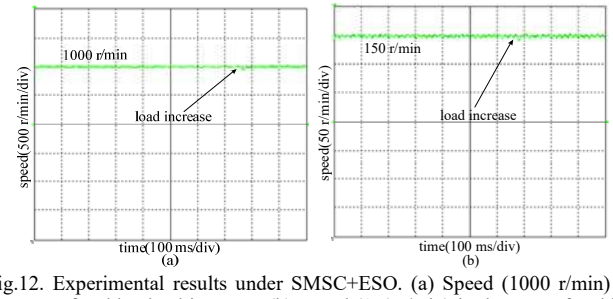

Fig.12. Experimental results under SMSC+ESO. (a) Speed (1000 r/min) in the case of sudden load increase. (b) Speed (150 r/min) in the case of sudden load increase.

From the experimental results of Fig.10 (a) and Fig.11 (a), it is obvious that when the 1.27 N·m load torque is added suddenly, the speed fluctuation under PI control is more obvious, and the dynamic settling time is about 80 ms. Relatively, as shown in Fig.11 (a), under the method of SMSC, when the load torque is changed suddenly, the speed fluctuation is smaller, moreover, its dynamic settling time is shorter. When the load torque increases to 1.27 N·m suddenly at 150 r/min, the same conclusion can still be obtained from the experimental results Fig.10 (b) and Fig.11 (b).

In addition, as from the experimental results of Fig.12, it is noted that the SMSC+ESO method has satisfying disturbance suppression ability compared with other method. Whether at high speed of 1000 r/min or at low speed of 150 r/min, the speed fluctuation under sudden load changes is smaller than other two control methods, which proves the correctness and effectiveness of the control method proposed in this paper.

V. Conclusion

A NSMRL has been proposed for optimizing the dynamic performance of PMSM speed regulation system. By establishing the simulation model of s function, it is proved fundamentally that compared with the traditional exponential reaching law and the reaching law in other reference, the reaching velocity of the proposed NSMRL in this paper is faster. Based on the NSMRL, a SMSC is designed to replace the conventional PI controller. Then, considering the large chattering phenomenon caused by high switching gains, an extended state observer based on hyperbolic tangent function is designed to estimate the load disturbance, and it is used as the feed-forward compensation added to the SMSC. The superiority of the proposed method (SMSC+ESO) has been confirmed through simulations and experiments, which results show that the designed method can obtain a satisfying performance with fast transient response, good disturbances rejection ability.

Reference

[1] T. Shi, Z. Wang and C. Xia, "Speed Measurement Error Suppression for PMSM Control System Using Self-Adaption Kalman Observer," in IEEE Transactions on Industrial Electronics, vol. 62, no. 5, pp. 2753-2763, May 2015.

[2] L. Sheng, W. Li, Y. Wang, M. Fan and X. Yang, "Sensorless Control of a Shearer Short-Range Cutting Interior Permanent Magnet Synchronous Motor Based on a New Sliding Mode Observer," in IEEE Access, vol. 5, pp. 18439-18450, 2017.

[3] A. K. Junejo, W. Xu, C. Mu and Y. Liu, "Improved Continuous Fast Terminal Sliding Mode Control for Speed Regulation of Sur-face-Mounted Permanent Magnet Synchronous Motor," 2018 21st International Conference on Electrical Machines and Systems (ICEMS), Jeju, 2018, pp. 93-98.

[4] S. Li and H. Gu, "Fuzzy Adaptive Internal Model Control Schemes for PMSM Speed-Regulation System," in IEEE Transactions on Industrial Informatics, vol. 8, no. 4, pp. 767-779, Nov. 2012.

[5] J. Li, H. P. Ren and Y. R. Zhong, "Robust Speed Control of Induction Motor Drives Using First-Order Auto-Disturbance Rejection Controllers," in IEEE Transactions on Industry Applications, vol. 51, no. 1, pp. 712-720, Jan.-Feb. 2015.

[6] M. Preindl and S. Bolognani, "Model Predictive Direct Torque Control With Finite Control Set for PMSM Drive Systems, Part 1: Maximum Torque Per Ampere Operation," in IEEE Transactions on Industrial Informatics, vol. 9, no. 4, pp. 1912-1921, Nov. 2013.

[7] Z. Ma, S. Saeidi and R. Kennel, "FPGA Implementation of Model Predictive Control With Constant Switching Frequency for PMSM Drives," in IEEE Transactions on Industrial Informatics, vol. 10, no. 4, pp. 2055-2063, Nov. 2014.

[8] X. Zhang, L. Sun, K. Zhao and L. Sun, "Nonlinear Speed Control for PMSM System Using Sliding-Mode Control and Disturbance Compensation Techniques," in IEEE Transactions on Power Electronics, vol. 28, no. 3, pp. 1358-1365, March 2013.

[9] C. Mu and H. He, "Dynamic Behavior of Terminal Sliding Mode Control," in IEEE Transactions on Industrial Electronics, vol. 65, no. 4, pp. 3480-3490, April 2018.

[10] C. Mu, W. Xu and C. Sun, "On Switching Manifold Design for Terminal Sliding Mode Control," Journal of the Franklin Institute, vol. 353, no. 7, pp. 1553-1572, May 2016.

[11] F. J. Lin, K. J. Yang, I. F. Sun and J. K. Chang, "Intelligent Position Control of Permanent Magnet Synchronous Motor Using Recurrent Fuzzy Neural Cerebellar Model Articulation Network," in IET Electric Power Applications, vol. 9, no. 3, pp. 248-264, 3 2015.

[12] V. Q. Leu, H. H. Choi and J. W. Jung, "Fuzzy Sliding Mode Speed Controller for PM Synchronous Motors With a Load Torque Observer," in IEEE Transactions on Power Electronics, vol. 27, no. 3, pp. 1530-1539, March 2012.

[13] C. K. Lai and Kuo-Kai Shyu, "A New Motor Drive Design for Incremental Motion System Via Sliding-mode Control Method," in IEEE Transactions on Industrial Electronics, vol. 52, no. 2, pp. 499-507, April 2005.

[14] X. Zhang, B. Hou and Y. Mei, "Deadbeat Predictive Current Control of Permanent-Magnet Synchronous Motors with Stator Current and Disturbance Observer," in IEEE Transactions on Power Electronics, vol. 32, no. 5, pp. 3818-3834, May 2017.

[15] Y. Jiang, W. Xu, C. Mu and Y. Liu, "Improved Deadbeat Predictive Current Control Combined Sliding Mode Strategy for PMSM Drive System," in IEEE Transactions on Vehicular Technology, vol. 67, no. 1, pp. 251-263, Jan. 2018.

[16] F. J. Lin, Y. C. Hung and M. T. Tsai, "Fault-Tolerant Control for Six-Phase PMSM Drive System via Intelligent Complementary Sliding-Mode Control Using TSKFNN-AMF," in IEEE Transactions on Industrial Electronics, vol. 60, no. 12, pp. 5747-5762, Dec. 2013.

[17] S. M. Mozayan, M. Saad, H. Vahedi, H. Fortin-Blanchette and M. Soltani, "Sliding Mode Control of PMSG Wind Turbine Based on Enhanced Exponential Reaching Law," in IEEE Transactions on Industrial Electronics, vol. 63, no. 10, pp. 6148-6159, Oct. 2016.

[18] J. Li, Y. Yang, C. Hua and X. Guan, "Fixed-time Backstepping Control Design for High-order Strict-feedback Non-linear Systems Via Terminal Sliding Mode," in IET Control Theory & Applications, vol. 11, no. 8, pp. 1184-1193, 5 12 2017.

[19] S. Di Gennaro, J. Rivera Domínguez and M. A. Meza, "Sensorless High Order Sliding Mode Control of Induction Motors With Core Loss," in IEEE Transactions on Industrial Electronics, vol. 61, no. 6, pp. 2678-2689, June 2014.

[20] Y. Feng, J. Zheng, X. Yu and N. V. Truong, "Hybrid Terminal Sliding-Mode Observer Design Method for a Permanent-Magnet Synchronous Motor Control System," in IEEE Transactions on Industrial Electronics, vol. 56, no. 9, pp. 3424-3431, Sept. 2009.

[21] D. Nojavanzadeh and M. Badamchizadeh, "Adaptive Fractional-order non-singular Fast Terminal Sliding Mode Control for Robot Manipulators," in IET Control Theory & Applications, vol. 10, no. 13, pp. 1565-1572, 8 29 2016.

[22] G. Sun, Z. Ma and J. Yu, "Discrete-Time Fractional Order Terminal Sliding Mode Tracking Control for Linear Motor," in IEEE Transactions on Industrial Electronics, vol. 65, no. 4, pp. 3386-3394, April 2018.

[23] Wasu S M , Sarode U B , Bhavalkar M P. "Speed Control of PMSM System Using Improved Reaching Law Based Sliding Mode Control and Disturbance Observer Technique," International Journal of Advanced Computer Research, 2013, 3(13).

[24] J. P. Mishra, X. Yu, M. Jalili and Y. Feng, "On Fast Terminal Sliding-mode Control Design for Higher Order Systems," IECON 2016 - 42nd Annual Conference of the IEEE Industrial Electronics Society, Florence, 2016, pp. 252-257.

[25] H. Liu and S. Li, "Speed Control for PMSM Servo System Using Predictive Functional Control and Extended State Observer," in IEEE Transactions on Industrial Electronics, vol. 59, no. 2, pp. 1171-1183, Feb. 2012.

[26] J. Han, "From PID to Active Disturbance Rejection Control," in IEEE Transactions on Industrial Electronics, vol. 56, no. 3, pp. 900-906, March 2009.
[27] Jianbo Su, Wenbin Qiu, Hongyu Ma and Peng-Yung Woo, "Calibration-free Robotic Eye-hand Coordination Based on an Auto Disturbance-rejection Controller," in IEEE Transactions on Robotics, vol. 20, no. 5, pp. 899-907, Oct. 2004.
[28] R. Miklosovic and Z. Gao, "A Robust Two-degree-of-freedom Control Design Technique and its Practical Application," Conference Record of the 2004 IEEE Industry Applications Conference, 2004. 39th IAS Annual Meeting., Seattle, WA, USA, 2004, pp. 1495-1502 vol.3.
[29] Y. Wu and Y. Ye, "Internal Model-Based Disturbance Observer With Application to CVCF PWM Inverter," in IEEE Transactions on Industrial Electronics, vol. 65, no. 7, pp. 5743-5753, July 2018.
[30] Y. X. Su, C. H. Zheng and B. Y. Duan, "Automatic Disturbances Rejection Controller for Precise Motion Control of Permanent-magnet Synchronous Motors," in IEEE Transactions on Industrial Electronics, vol. 52, no. 3, pp. 814-823, June 2005.
[31] Weibing Gao and J. C. Hung, "Variable Structure Control of Nonlinear Systems: a New Reach," in IEEE Transactions on Industrial Electronics, vol. 40, no. 1, pp. 45-55, Feb 1993.
[32] A. Scottedward Hodel and C. E. Hall, "Variable-structure PID Control to Prevent Integrator Windup," in IEEE Transactions on Industrial Electronics, vol. 48, no. 2, pp. 442-451, April 2001.

Yaoqiang Wang (S'12-M'16) received the B.Sc. degree in Measurement & Control Technology and Instruments from the Hangzhou Dianzi University, Hangzhou, China, in 2006, and the M.Sc. and Ph.D. degrees in Electrical Engineering from the Harbin Institute of Technology, Harbin, China, in 2008 and 2013, respectively.

He is currently working as an Associate Professor with the School of Electrical Engineering, Zhengzhou University, Zhengzhou, China. He has authored more than 30 technical papers published in journals and conference proceedings. His research interests include power conversion & control technique and its applications in distributed generation, motor drive and flexible power transmission & distribution, etc.

Yutao Feng received the B.Sc. degree in Electrical Engineering and Its Automation from the Shandong University of Science and Technology, Qingdao, China, in 2016, and the M.Sc. degree in Electrical Engineering from the Zhengzhou University, Zhengzhou, China, in 2019.

He is currently working as a Researcher with the China Aviation Optical-Electrical Technology Co., Ltd., Luoyang, China. His research interests include power electronics and electric machine drives.

Xiaoguang Zhang (M'15) received the B.Sc. degree in Electrical Engineering from the Heilongjiang Institute of Technology, Harbin, China, in 2007, and the M.Sc. and Ph.D. degrees in Electrical Engineering from the Harbin Institute of Technology, in 2009 and 2014, respectively.

He is currently a Distinguished Professor with the North China University of Technology. From 2012 to 2013, he was a Research Associate at Wisconsin Electric Machines and Power Electronics Consortium (WEMPEC), University of Wisconsin–Madison, Madison. He has published more than 40 technical papers in the area of motor drives. His current research interests include power electronics and electric machine drives.

Jun Liang (M'02–SM'12) received the B.Sc. degree from the Huazhong University of Science and Technology, Wuhan, China, in 1992, and the M.Sc. and Ph.D. degrees from the China Electric Power Research Institute (CEPRI), Beijing, China, in 1995 and 1998, respectively, all in Electrical Engineering and Its Automation.

From 1998 to 2001, he was a Senior Engineer with CEPRI. From 2001 to 2005, he was a Research Associate with Imperial College London, London, U.K. From 2005 to 2007, he was with the University of Glamorgan as a Senior Lecturer. He is currently a Professor with the School of Engineering, Cardiff University, Cardiff, U.K. He has been appointed as an Adjunct Professor at the Zhengzhou University, Zhengzhou, China, since 2019. His research interests include power system stability and control, DC grids, power electronics, and renewable power generation.